Journal of Sound and Vibration 329 (2010) 4719–4739

Contents lists available at ScienceDirect

Journal of Sound and Vibration

journal homepage: www.elsevier.com/locate/jsvi

# The effect of turbulence damping on acoustic wave propagation in tubes

Magnus Knutsson [a,b,*], Mats Åbom [b]

[a] Volvo Car Coporation, SE-40531 Göteborg, Sweden
[b] KTH CICERO, The Marcus Wallenberg Laboratory, Royal Institute of Technology, SE-100 44 Stockholm, Sweden

ARTICLE INFO

*Article history:*
Received 24 April 2009
Received in revised form
10 March 2010
Accepted 16 May 2010
Handling Editor: R.J. Astley
Available online 12 June 2010

ABSTRACT

The attenuation of sound due to the interaction between a low Mach number turbulent boundary layer and acoustic waves can be significant at low frequencies or in narrow tubes. In a recent publication by the present authors the acoustics of charge air coolers for passenger cars has been identified as an interesting application where turbulence attenuation can be of importance. Favourable low-frequency damping has been observed that could be used for control of the in-duct sound that is created by the engine gas exchange process. Analytical frequency-dependent models for the eddy viscosity that controls the momentum and thermal boundary layers are available but are restricted to thin acoustic boundary layers. For cases with cross-sections of a few millimetres a model based on thin acoustic boundary layers will not be applicable in the frequency range of interest.

In the present paper a frequency-dependent axis-symmetric numerical model for interaction between turbulence and acoustic waves is proposed. A finite element scheme is used to formulate the time harmonic linearized convective equations for conservation of mass, momentum and energy into one coupled system of equations. The turbulence is introduced with a linear model for the eddy viscosity that is added to the shear viscosity. The proposed model is validated by comparison with experimental data from the literature.



## 1. Introduction

The subject of sound propagation in narrow tubes has been investigated by numerous researchers throughout the years. Kirchhoff [1] found that the dissipation of sound waves was a result of viscous and thermal effects close to the walls. He also proposed a description in the form of a complex transcendental equation for the case of a fluid with no incompressible flow present. An approximate solution to a simplified version of Kirchhoff's equation was obtained by Zwikker and Kosten [2] for circular geometries. Research efforts by several consecutive authors were summarized by Tijdeman [3]. None of this early work, however, treated the effect of a steady mean flow. Peat [4] and Ih et al. [5] have thereafter proposed variational solutions assuming a parabolic steady velocity distribution and neglecting the influence of radial velocity components. A numerical solution scheme based on the same assumptions was proposed by Astley and Cummings [6] and included non-circular geometries. Jeong and Ih [7] and Willatzen [8] studied the influence of the radial velocity term.

* Corresponding author at: KTH CICERO, The Marcus Wallenberg Laboratory for Sound and Vibration Research, Department of Aeronautical and Vehicle Engineering, KTH, SE-100 44 Stockholm, Sweden. Tel.: +46 73 770 9972/+46 31 325 4064; fax: +46 8 790 61 22.
*E-mail addresses:* magnuskn@kth.se, mknutsso@volvocars.com (M. Knutsson).

0022-460X/$ - see front matter © 2010 Elsevier Ltd. All rights reserved.
doi:10.1016/j.jsv.2010.05.018

While assuming a constant steady flow and the Zwikker and Kosten [2] simplifications Dokumaci derived solutions for ducts with circular as well as rectangular cross-sections [9,10]. The effect of axial pressure and temperature gradients has been treated by Peat [11], Peat and Kirby [12], and Dokumaci [13]. Two important conclusions from those works is that good correspondence can be obtained if a non-circular tube is modelled as a circular duct with the same hydraulic diameter and that the radial velocity term might affect the results but just to a small extent.

The effect of attenuation of pulsations through interaction with turbulence has mainly been investigated by the fluid mechanics community. Large amplitude velocity-oscillations in ducted flow was investigated experimentally, e.g. by Tardu et al. [14]. Examples of recent efforts that use Large-Eddy simulations as a tool to study different aspects of the phenomena including acoustic waves are the work by Scotti and Piomelli [15] and by Comte et al. [16]. An example of an early attempt to model the effect of turbulence damping of acoustic waves in pipe flow is the work by Ingard and Singhal [17] where a crude model of the dissipation was introduced as a modified wavenumber. Other attempts to model acoustic wave propagation in turbulent pipe flows were for instance reported by Ronneberger and Ahrens [18], Mankbadi and Liu [19] and Peters et al. [20]. Detailed experimental data was also provided in Refs. [18,20] and by Allam and Åbom [21]. From those studies it has been concluded that damping is achieved if the thickness of the acoustic boundary layer is larger than the viscous sublayer. A frequency-dependent model of the effective turbulent boundary layer viscosity was proposed by Howe [22]. From assuming that the thicknesses of the boundary layers are much smaller than the acoustic wavelength he proposed to replace the layers by an acoustic impedance and thereafter solve an inhomogeneous wave equation. This model is probably the most complete analytical model so far concerning sound–turbulence interaction within circular ducts. However, it is restricted to thin acoustic boundary layers, small Mach numbers and assumes a uniform mean core flow. An improved variant of Howe's model, that was proposed recently by Dokumaci [23], is based on the assumption of parallel sheared mean core flow. By taking into account the effect of the mean velocity profile, this model will allow thicker sublayers than Howe's model but still assumes negligible mean flow effects in the sublayer. Dokumaci also used the model in Ref. [23] to extract a two-port, which also was done at the same time by the present authors in Ref. [24], however, using the original variant of Howe's model.

In the paper by the present authors [24], where the acoustics of charge air coolers was investigated, favourable low frequency damping due to interaction between turbulent boundary layers and acoustic waves was observed. However, as the cooling tubes were rather narrow no available model gave satisfying predictions of this phenomenon and hence the need for an improved model was enlightened. In the present investigation a numerical study is presented where the finite element scheme proposed by Astley and Cummings [6] is reformulated into cylindrical coordinates and extended to account for the interaction between sound and turbulence. The absorption due to the turbulence is introduced with a linear model for the eddy viscosity that is added to the shear viscosity. This turbulence model, originating from the work by Prandtl, has earlier been used by Howe [22]. The proposed numerical model in the present investigation has been used to inversely calculate the spatial distribution of the turbulence damping within the boundary layer for three test cases presented by Peters et al. [20] and Allam and Åbom [21]. As a result, two modified versions of the empirical formula by Howe [22] for the thickness of the viscous sublayer interacting with acoustic waves in the upstream and downstream direction, respectively, are proposed for use with the current formulation. These new equations include the effect of a convective mean flow and the curvature of the duct wall; hence they will yield improved estimates for smaller Stokes numbers as long as the flow is turbulent. The small amount of extra damping, that has been observed in the experimental data at low Mach numbers in the upstream direction in addition to the purely viscothermal, and which has been neglected so far [22] has been found to coincide in the three test cases. To include this effect a simple empirical model is proposed for use together with the finite element scheme in order to yield estimates better in accordance with the observed data.

## 2. Sound propagation in tubes including viscous and thermal effects

### 2.1. General

When analysing sound propagation in tubes it can often be assumed that the wave front is uniform throughout the cross-section. This assumption is limited to those cases where the frequency $f$ under consideration is below the cut-on frequency for the first non-plane mode. For circular cross-sections this limit is given by the first zero of $J'_1$, the derivative of the Bessel function of the first kind, as [25]

$$k_0 R < 1.84 \quad \text{or} \quad f < \frac{1.84 c_0}{2R\pi}, \tag{1}$$

where $R$ is the radius of the tube, $k_0 = \omega/c_0$ the wavenumber, $\omega$ the angular frequency, $c_0 = \sqrt{\gamma p_0/\rho_0}$ the isentropic speed of sound, $\gamma$ the ratio of specific heat and $p_0$ and $\rho_0$ are the pressure and density of the undisturbed gas, respectively. In situations where a detailed description of the damping is of importance the dissipative effect due to viscosity and heat conduction must be taken into account. The viscothermal damping, $\alpha_{\text{fluid}}$ (the negative imaginary part of the wavenumber) in the fluid itself is (see Ref. [25] or [26])

$$\alpha_{\text{fluid}} = \frac{\omega^2 \mu}{2\rho_0 c_0^3}\left(\frac{4}{3} + \frac{\mu_v}{\mu} + \frac{\gamma - 1}{\xi^2}\right), \tag{2}$$

where $\mu$ is the coefficient of shear viscosity, $\mu_v$ the expansion coefficient of viscosity and $\xi^2=\mu C_p/\kappa_{\mathrm{th}}$ the Prandtl number. The specific heat at constant pressure is $C_p$ and the thermal conductivity is $\kappa_{\mathrm{th}}$. For the case of sound propagation in ducts the dissipation due to viscous and thermal effects at the boundaries are much larger than those in the fluid itself. The early model for sound propagation in circular tubes by Kirchhoff [1] from 1868 includes the effect of viscosity as well as heat conduction. Kirchhoff himself formulated a solution for sound propagation in wide ducts yielding a modified wavenumber as

$$k=\frac{\omega}{c_0}\left[1+\frac{1-i}{\sqrt{2}s}\left(1+\frac{\gamma-1}{\xi}\right)-\frac{i}{s^2}\left(1+\frac{\gamma-1}{\xi}-\frac{\gamma}{2}\frac{\gamma-1}{\xi^2}\right)\right], \tag{3}$$

where $s=R\sqrt{\omega/\nu}$ is a shear wavenumber often referred to as the Stokes number and $\nu=\mu/\rho_0$ is the kinematic viscosity. From Eq. (3) it follows that the damping $\alpha_0$ in a quiescent fluid is

$$\alpha_0=\frac{\omega}{c_0}\left[\frac{1}{\sqrt{2}s}\left(1+\frac{\gamma-1}{\xi}\right)+\frac{1}{s^2}\left(1+\frac{\gamma-1}{\xi}-\frac{\gamma}{2}\frac{\gamma-1}{\xi^2}\right)\right]. \tag{4}$$

The $1/s^2$ term is very small and is therefore often neglected. In the present work it is, however, retained but the damping of the fluid itself can as noted above be neglected. Several authors have treated solutions to Kirchhoff's equation. One important early example is the approximate solution to a simplified version of Kirchhoff's equation that was found by Zwikker and Kosten [2] for circular geometries. Their solution is only dependent on the shear wavenumber and is also known as the "low reduced frequency solution" [3] since it is only valid for cases where $k_0R\ll 1$ and $k_0R/s\ll 1$.

The evolution of catalytic converters during the latest 20 years inspired several authors to develop improved models that include the effect of convective mean flow [4–13]. One model that appears to be particularly useful for practical applications is the model by Dokumaci in Ref. [9]. By approximating the mean flow profile as constant over the tube cross-section he showed that the simplified equations by Zwikker and Kosten could be solved analytically for the convective circular case. In a later paper [10], he extended the model in Ref. [9] to include rectangular cross-sections by expanding the solution in terms of a double Fourier sine series. Astley and Cummings presented in Ref. [6], a numerical finite element solution scheme based on the simplifications by Zwikker and Kosten that was able to predict solutions for arbitrary shaped cross-sections for arbitrary mean flow profiles. Both Dokumaci's and Astley and Cummings' findings will be used extensively in the current work. For the derivation of Dokumaci's solution the reader is referred to his paper [9]. The solution scheme formulated in [6] will be summarized here; however, reformulated for the axis-symmetric circular case in the form of an axis-symmetric ring-element.

### 2.2. Formulation of the linear governing equations

The treatment of linear acoustic waves is normally based on linearization of the equations for conservation of mass and momentum together with an assumption of no losses and isentropic changes of state, leading to the classical wave equation in a homogenous fluid at rest. For situations where losses are of importance the linearized equation for conservation of energy must be included. Since the velocity appears in all equations they are coupled and a full treatment of the problem requires that they are solved together. For the case of sound waves, below the cut-on frequency for the first non-plane mode, travelling in a tube where an incompressible parallel mean flow is present the conservation equations can be linearized, assuming small perturbations from a steady mean value and neglecting second order terms, using $\mathbf{u}=\bar{\mathbf{u}}+\mathbf{u}'$, $p=p_0+p'$, $T=T_0+T'$ and $\rho=\rho_0+\rho'$. The acoustic velocity $\mathbf{u}'$ comprises $u_x'$, $u_r'$ and $u_\theta'$ for each direction, and the incompressible mean flow $\bar{\mathbf{u}}$ is $U_0(r)$ in the axial direction and zero in the other two directions. Following Ref. [6] the equation for conservation of mass using the above mentioned simplifications, while assuming that the axial pressure drop is small becomes

$$\frac{\partial\rho'}{\partial t}+\rho_0\nabla\cdot\mathbf{u}'+U_0\frac{\partial\rho'}{\partial x}=0. \tag{5}$$

For a circular cross section with radius $R$, rigid tube walls together with Gauss' divergence theorem yields the following integral form for harmonic waves [$\exp(i\omega t)$]:

$$\int_0^{2\pi}\int_0^R\left[\left(i\omega+U_0\frac{\partial}{\partial x}\right)\rho'+\rho_0\frac{\partial u_x'}{\partial x}\right]r\,\mathrm{d}r\,\mathrm{d}\theta=0. \tag{6}$$

The linearized equation for conservation of momentum, using the same simplifications, becomes

$$\rho_0\left[\frac{\partial\mathbf{u}'}{\partial t}+(\bar{\mathbf{u}}\cdot\nabla)\mathbf{u}'+(\mathbf{u}'\cdot\nabla)\bar{\mathbf{u}}\right]=-\nabla p'+\mu\left[\nabla^2\mathbf{u}'+\frac{1}{3}\nabla(\nabla\cdot\mathbf{u}')\right]. \tag{7}$$

For the axis-symmetric case (no tangential variations) Eq. (7) can be reformulated, using cylindrical coordinates, to become

$$\rho_0\left[\left(i\omega+U_0\frac{\partial}{\partial x}\right)u_x'+u_r'\frac{\partial U_0}{\partial r}\right]=-\frac{\partial p'}{\partial x}+\mu\left[\frac{\partial^2u_x'}{\partial x^2}+\frac{\partial^2u_x'}{\partial r^2}+\frac{1}{r}\frac{\partial u_x'}{\partial r}+\frac{1}{3}\left(\frac{\partial^2u_x'}{\partial x^2}+\frac{\partial^2u_r'}{\partial x\partial r}+\frac{1}{r}\frac{\partial u_r'}{\partial x}\right)\right] \tag{8}$$

and

$$\rho_0\left(i\omega+U_0\frac{\partial}{\partial x}\right)u_r'=-\frac{\partial p'}{\partial r}+\mu\left[\frac{\partial^2 u_r'}{\partial x^2}+\frac{\partial^2 u_r'}{\partial r^2}+\frac{1}{r}\frac{\partial u_r'}{\partial r}-\frac{u_r'}{r^2}+\frac{1}{3}\left(\frac{\partial^2 u_x'}{\partial x\partial r}+\frac{\partial^2 u_r'}{\partial r^2}+\frac{1}{r}\frac{\partial u_r'}{\partial r}-\frac{u_r'}{r^2}\right)\right], \tag{9}$$

in the axial and radial direction, respectively. Here, $u_x'$ and $u_r'$ are the acoustic velocity perturbations in the axial and radial directions, respectively. Using the conventional boundary layer approximation that the radial velocity is much smaller than the axial and that radial changes are much larger than axial ($u_r' \gg u_x'$ and $\partial/\partial r \gg \partial/\partial x$) Eqs. (8) and (9) simplifies to [4–6]

$$\rho_0\left(i\omega+U_0\frac{\partial}{\partial x}\right)u_x'=-\frac{\partial p'}{\partial x}+\mu\left(\frac{\partial^2 u_x'}{\partial r^2}+\frac{1}{r}\frac{\partial u_x'}{\partial r}\right) \tag{10}$$

and

$$\frac{\partial p'}{\partial r}=0, \tag{11}$$

respectively. The linearized equation for conservation of energy is [25]

$$\rho_0 C_p\left(\frac{\partial T'}{\partial t}+\overline{\mathbf{u}}\cdot\nabla T'\right)=\frac{\partial p'}{\partial t}+\overline{\mathbf{u}}\cdot\nabla p'+\kappa_{\mathrm{th}}\nabla_\perp^2 T'+\rho_0\phi, \tag{12}$$

where the ideal gas relation $\beta_0 T_0=1$ has been used and it has been assumed that there are no pressure or temperature drop in the axial direction. The dissipation function is

$$\phi=2\nu\left(e_{ij}e_{ij}-\frac{1}{3}\Delta^2\right), \tag{13}$$

where $e_{ij}$ is the rate of strain tensor and the local rate of expansion is $\Delta=\nabla\cdot\mathbf{u}$. Using the previous assumptions Eq. (12) simplifies to

$$\rho_0 C_p\left(i\omega+U_0\frac{\partial}{\partial x}\right)T'=\left(i\omega+U_0\frac{\partial}{\partial x}\right)p'+\kappa_{\mathrm{th}}\left(\frac{\partial^2 T'}{\partial r^2}+\frac{1}{r}\frac{\partial T'}{\partial r}\right)+2\mu\frac{\partial U_0}{\partial r}\frac{\partial u_x'}{\partial r}. \tag{14}$$

Using the ideal gas law the linearized equation of state is obtained as

$$\frac{p'}{p_0}=\frac{\rho'}{\rho_0}+\frac{T'}{T_0}. \tag{15}$$

It should be pointed out that the acoustic radial velocity term $u'_r$ is omitted in Eqs. (10) and (14) with reference to the argumentation in [4,6–8] that the effects are small.

### 2.3. The dimensionless eigenvalue problem

Following the procedure in Ref. [6], however, here using cylindrical coordinates, the following ansatz can be used to obtain a plane wave type of solution to Eqs. (6), (10) and (14):

$$u_x'=c_0 u^*(r^*)\exp(i\omega t-ik_0\Gamma x), \tag{16}$$

$$p'=p_0 p^*\exp(i\omega t-ik_0\Gamma x), \tag{17}$$

$$T'=T_0 T^*(r^*)\exp(i\omega t-ik_0\Gamma x), \tag{18}$$

where $\Gamma$ is a dimensionless axial wavenumber. The dimensionless amplitude coefficients $u^*$, $p^*$ and $T^*$ for the acoustic velocity, pressure and temperature, respectively, have been introduced in order to simplify the solution of the coupled equations. The radial coordinate has been non-dimensionalized using the tube radius as $r^*=r/R$ and is valid within the domain $0<r^*<1$. The equation of state yields

$$\frac{\rho'}{\rho_0}=(p^*-T^*)\exp(i\omega t-ik_0\Gamma x). \tag{19}$$

Substitution of Eqs. (16)–(19) into Eqs. (6), (10) and (14) yields the following conservation equations:
Mass

$$\int_0^1 [i(1-\Gamma M)(p^*-T^*)-i\Gamma u^*]r^*\,\mathrm{d}r^*=0. \tag{20}$$

Momentum

$$\frac{\gamma}{s^2}\left(\frac{\partial^2 u^*}{\partial r^{*2}}+\frac{1}{r^*}\frac{\partial u^*}{\partial r^*}\right)-i\gamma(1-\Gamma M)u^*+i\Gamma p^*=0. \tag{21}$$

Energy

$$\frac{\gamma}{\gamma-1}\frac{1}{s^2\xi^2}\left(\frac{\partial^2 T^*}{\partial r^{*2}}+\frac{1}{r^*}\frac{\partial T^*}{\partial r^*}\right)-\frac{i\gamma}{\gamma-1}(1-\Gamma M)T^*+i(1-\Gamma M)p^*+\frac{2\gamma}{s^2}\frac{\partial M}{\partial r^*}\frac{\partial u^*}{\partial r^*}=0. \tag{22}$$

### 2.4. Formulation of the finite element matrices

The finite element process is based on finding an approximate solution (trial solution) of, for this particular case, the velocity and temperature fields in the form

$$u^*=\sum_{i=1}^{n}u_i{}^*\phi_i(r^*),\quad T^*=\sum_{i=1}^{n}T_i{}^*\phi_i(r^*), \tag{23}$$

where $\phi_i$ are the known shape functions, which must be able to satisfy the boundary conditions individually, and $u_i^*$ and $T_i^*$ are unknown coefficients. The boundary conditions are zero acoustic velocity and temperature at the duct wall and zero derivatives at the centre of the duct as

$$u^*=T^*=0 \text{ at } r^*=1,\quad \frac{\partial u^*}{\partial r^*}=\frac{\partial T^*}{\partial r^*}=0 \text{ at } r^*=0. \tag{24}$$

The plane wave ansatz for the pressure in Eq. (17) gives

$$p^*=p_1^*=\text{constant}. \tag{25}$$

Substitution of Eqs. (23) and (25) into the integral equation (20) yields

$$\frac{i}{2}(1-\Gamma\overline{M})p^*-i(\boldsymbol{\varphi}^T-\Gamma\boldsymbol{\varphi}_m^T)\mathbf{T}^*-i\Gamma\boldsymbol{\varphi}^T\mathbf{u}^*=0, \tag{26}$$

where

$$\boldsymbol{\varphi}^T=\int_0^1\begin{bmatrix}r^*\phi_1\\-\\-\\r^*\phi_n\end{bmatrix}\mathrm{d}r^*,\quad \boldsymbol{\varphi}_m^T=\int_0^1\begin{bmatrix}r^*M\phi_1\\-\\-\\r^*M\phi_n\end{bmatrix}\mathrm{d}r^*, \tag{27}$$

$$\mathbf{u}^*=\begin{bmatrix}u_1{}^*\\-\\-\\u_n{}^*\end{bmatrix},\quad \mathbf{T}^*=\begin{bmatrix}T_1{}^*\\-\\-\\T_n{}^*\end{bmatrix}\quad \text{and } p^*=[p_1{}^*]. \tag{28}$$

The Mach number of the incompressible flow averaged over the cross-section, that is required in Eq. (26) is

$$\overline{M}=2\int_0^1 M(r^*)r^*\,dr^*. \tag{29}$$

The Galerkin method applied to Eq. (21) together with the divergence theorem yields

$$-\frac{\gamma}{s^2}\int_0^1\frac{\partial\phi_j}{\partial r^*}\frac{\partial u^*}{\partial r^*}r^*\mathrm{d}r^*-i\gamma\int_0^1(1-\Gamma M)\phi_j u^* r^*\mathrm{d}r^*+i\int_0^1\Gamma\phi_j p^* r^*\mathrm{d}r^*=0, \tag{30}$$

where $j=1,2,\ldots,n$. Substitution of the expressions for $p^*$ and $u^*$ from Eqs. (23) and (25) in (30) yields

$$\frac{\gamma}{s^2}\mathbf{B}\mathbf{u}^*+i\gamma(\mathbf{A}-\Gamma\mathbf{A}_m)\mathbf{u}^*-i\Gamma\boldsymbol{\varphi}p^*=\mathbf{0}. \tag{31}$$

Here $\mathbf{A}$, $\mathbf{B}$ and $\mathbf{A}_m$ are $n\times n$ matrices where $n$ is the number of nodes and the $j$–$k$th components are given by

$$[\mathbf{A}]_{jk}=\int_0^1\phi_j\phi_k r^*\,dr^*,\quad [\mathbf{B}]_{jk}=\int_0^1\frac{\partial\phi_j}{\partial r^*}\frac{\partial\phi_k}{\partial r^*}r^*\,dr^*, \tag{32}$$

$$[\mathbf{A}_m]_{jk}=\int_0^1 M\phi_j\phi_k r^*\,dr^*. \tag{33}$$

The same procedure on the energy equations yields

$$\frac{\gamma}{\gamma-1}\frac{1}{s^2\xi^2}\mathbf{B}\mathbf{T}^*+\frac{i\gamma}{\gamma-1}(\mathbf{A}-\Gamma\mathbf{A}_m)\mathbf{T}^*-\frac{2\gamma}{s^2}\mathbf{C}_m\mathbf{u}^*-i(\boldsymbol{\varphi}-\Gamma\boldsymbol{\varphi}_m)p^*=\mathbf{0}. \tag{34}$$

The $\mathbf{C}_m$-term due to the fluctuating dissipation function is

$$[\mathbf{C}_m]_{jk} = \int_0^1 \phi_j \frac{\partial M}{\partial r^*} \frac{\partial \phi_k}{\partial r^*} r^* \mathrm{d}r^*. \tag{35}$$

When a mean flow is present Eqs. (26), (31) and (35) are coupled and need to be solved together. Here, they are solved using the following matrix equation:

$$\left[ \begin{bmatrix} i/2 & \mathbf{0} & -i\boldsymbol{\varphi}^T \\ \mathbf{0} & \gamma\mathbf{B}/s^2 + i\gamma\mathbf{A} & \mathbf{0} \\ -i\boldsymbol{\varphi} & -\frac{2\gamma}{s^2}\mathbf{C}_m & \frac{\gamma}{\gamma-1}\left[\frac{\mathbf{B}}{s^2\xi^2} + i\mathbf{A}\right] \end{bmatrix} - \Gamma \begin{bmatrix} i\overline{M}/2 & i\boldsymbol{\varphi}^T & -i(\boldsymbol{\varphi}_m)^T \\ i\boldsymbol{\varphi} & i\gamma\mathbf{A}_m & \mathbf{0} \\ -i\boldsymbol{\varphi}_m & \mathbf{0} & \frac{i\gamma}{\gamma-1}\mathbf{A}_m \end{bmatrix} \right] \begin{bmatrix} p^* \\ \mathbf{u}^* \\ \mathbf{T}^* \end{bmatrix} = \begin{bmatrix} 0 \\ \mathbf{0} \\ \mathbf{0} \end{bmatrix}. \tag{36}$$

Here, $\mathbf{0}$ indicates a zero matrix of appropriate size.

### 2.5. Shape functions and discretisation considerations

The procedure of establishing the shape functions in Eq. (23) is well described in any text book describing the finite element method, i.e. Ref. [27]. In the present investigation three node parabolic Lagrange elements with symmetric positioned middle node are used. The three shape functions for an element of length $L^e$ are

$$\phi_1^e = \frac{2}{(L^e)^2}\left(\eta - \frac{L^e}{2}\right)(\eta - L^e), \tag{37}$$

$$\phi_2^e = -\frac{4}{(L^e)^2}\eta(\eta - L^e), \tag{38}$$

$$\phi_3^e = \frac{2}{(L^e)^2}\eta\left(\eta - \frac{L^e}{2}\right), \tag{39}$$

where $\eta$ is the local radial coordinate of the element. In the calculation of the system matrices the integration is performed analytically, a procedure that would have to be carried out numerically for isoparametric 2D elements. The nodal discretisation must be able to represent the shear waves in the velocity and temperature fields with large gradients close to the boundaries. All meshes used in the investigation are therefore strongly biased with the finest resolution close to the wall.

## 3. Dissipation by turbulence

### 3.1. General

When a turbulent mean flow is present in a tube the unsteady transport of momentum, which creates the turbulent shear stress, can be modulated by acoustic waves. This modulation will cause an extra mixing, that is mainly important where the gradients of the acoustic particle velocity are large, which will result in a conversion of acoustic energy into turbulent energy and increased acoustic losses. The numerical approach described in the previous section is here modified in order to improve the model for turbulence damping of sound in tubes proposed by Howe in Ref. [22] and include the effect of convection plus allow for thicker acoustic boundary layers.

### 3.2. Turbulence model

The structure of the boundary layer of a turbulent flow is well documented in the literature and will not be described in detail here. Basically it consists of the viscous sublayer, the transition zone and the turbulent region [28–30]. The velocity distribution and the thickness of the layers are controlled by the parameter $y^+ = u_\tau y/\nu$, where $u_\tau$ is the wall-friction velocity defined as $u_\tau = \sqrt{\tau_w/\rho}$, $\tau_w$ is the wall shear stress and $y$ is the distance from the wall. Several experimental investigators have shown that within the viscous sublayer close to a smooth rigid wall the axial velocity distribution is approximately determined by

$$\frac{U_0}{u_\tau} = \frac{u_\tau y}{\nu} \tag{40}$$

and in the turbulent region as

$$\frac{U_0}{u_\tau} = \frac{1}{\kappa}\ln\left(\frac{u_\tau y}{\nu}\right) + \text{constant}, \tag{41}$$

where $\kappa \approx 0.41$ is the von Kármán constant and the constant is approximately 4.9. In the transition zone between the viscous sublayer and the turbulent region a gradual transition between Eqs. (40) and (41) has been reported. There is, however, no precise limit between the layers but experiments suggests that the gradual transition from laminar to turbulent flow takes place in the zone where $5 < u_\tau y/\nu < 30$. Combining Eqs. (40) and (41) while solving for $y^+$ gives an approximation of the nominal viscous sublayer thickness as $y^+ = u_\tau y/\nu \approx 10.7$. The friction velocity $u_\tau$ is here determined from the empirical pipe flow formula [29]

$$\frac{U_0}{u_\tau} = \frac{1}{\kappa}\ln\left(\frac{u_\tau R}{\nu}\right) + 2.0. \tag{42}$$

Based on earlier experimental investigations on the subject [18–20] there is a discussion in Ref. [22] about damping of acoustical waves defined by the relation of the thickness of the acoustical sublayer to the thickness of the viscous sublayer for an oscillating turbulent mean flow. Several authors have reported that for low frequencies when the acoustic boundary layer extends far out in the turbulent region significant damping is achieved [18–20]. Hence, for high frequencies, when the acoustic boundary layer is very thin and stays within the viscous sublayer, there is no effect of turbulence on the acoustic dissipation. In the region where the acoustic sublayer is about twice as thick as the viscous sublayer the damping will be controlled by both viscous effects as well as turbulence interaction [22]. The identification of this region is important for the discussion later in this paper of a modified version of the model by Howe [22]. The frequency-dependent thickness of the acoustic boundary layer, or the viscous penetration depth, for a sound wave passing over an infinite, smooth plate located at $y=0$ in a medium where there is no mean flow present can be derived from the boundary layer equation

$$\frac{\partial u_x'}{\partial t} = -\frac{1}{\rho_0}\frac{\partial p'}{\partial x} + \nu\frac{\partial^2 u_x'}{\partial y^2}, \tag{43}$$

where $x$ is parallel to the plate. The well known solution for harmonic waves [$\exp(i\omega t)$] is [25]

$$u_x' = \frac{p'}{\rho_0 c_0}\left[1 - e^{y(i-1)\sqrt{\omega/(2\nu)}}\right] \tag{44}$$

which yields the thickness of the acoustic boundary layer as [25]

$$\delta_A = \sqrt{2\nu/\omega}. \tag{45}$$

When there is a uniform mean flow $U_0$ present, Eq. (43) is modified to

$$\left(i\omega + U_0\frac{\partial}{\partial x}\right)u_x' = -\frac{1}{\rho_0}\frac{\partial p'}{\partial x} + \nu\frac{\partial^2 u_x'}{\partial y^2}. \tag{46}$$

In Ref. [9] Dokumaci assumed a uniform profile and was able to extract an analytical solution for convective sound in a circular tube. For the case of a sound wave passing an infinite plate the solution to Eq. (46) can, from using the Dokumaci approximation with a constant mean flow, be obtained as

$$u_x' = \frac{p'}{\rho_0 c_0(1-M)}\left\{1 - e^{y(i-1)\sqrt{\omega/[2\nu(1-M)]}}\right\}. \tag{47}$$

It is obvious that the thickness of the acoustic sublayer is different when an incompressible mean flow is superimposed, but also that it will be different for waves propagating up- and downstream the flow. For the case of a circular tube Ref. [9] gives the relation between acoustic velocity and pressure as

$$u_x' = \frac{p'\Gamma}{\rho_0 c_0(1-\Gamma M)}\left\{1 - \frac{J_0\left[r(i-1)\sqrt{\omega(1-\Gamma M)/(2\nu)}\right]}{J_0\left[R(i-1)\sqrt{\omega(1-\Gamma M)/(2\nu)}\right]}\right\}, \tag{48}$$

where $\Gamma$ is a dimensionless, imaginary axial wavenumber, that has different sign and value for up- and downstream propagation, and $J_0$ the Bessel function of the first kind. The thickness of the acoustic boundary layer is no longer intuitively defined here. In the present work it is proposed to use the normalised admittance $H = \rho_0 c_0 u_x'/p'$ in the plane, unconvected case and use this value in the convective bounded case to calculate the corresponding thicknesses of the acoustic boundary layers. Since we are interested in finding half the thickness of the acoustic sublayer $\delta_{A\phi M\pm}/2$ (where the index $\phi$ refers to the circular case and $M\pm$ to the convective case for down- or upstream travelling waves, respectively) we get the following equation:

$$\left|1 - e^{(i-1)/2}\right| = \left|\frac{\Gamma}{(1-\Gamma M)}\left\{1 - \frac{J_0\left[\frac{\delta_{A\phi M\pm}}{2}(i-1)\sqrt{\omega(1-\Gamma M)/(2\nu)}\right]}{J_0\left[R(i-1)\sqrt{\omega(1-\Gamma M)/(2\nu)}\right]}\right\}\right|, \tag{49}$$

that can be solved by iteration. However, first $\Gamma$ must be calculated, a task that can be carried out iteratively as is described in Ref. [9].

Fig. 1 exemplifies the solution to Eq. (49). It can clearly be seen that for this particular case the difference between the infinite plate solution and the cylindrical solution without incompressible mean flow is very small. This difference is dependent on the Stokes number and will become much larger for low Stokes numbers when the thickness of the acoustic boundary layer is of the same order of magnitude as the tube radius. For the convective solutions it can be stated that the thickness of the acoustic boundary layer is thinner for upstream propagating waves and thicker for downstream propagating waves (indicated by the two vertical lines). This effect is controlled by the Mach number.

Based on the discussion above it can now be concluded that the state when the edge of the viscous sublayer coincides with middle of the acoustic sublayer is defined by the Stokes number, the Mach number and the direction of flow. In Ref. [22] Howe described the state when the viscous and thermal effects as well as the effects from turbulence diffusion are significant using a critical frequency. From assuming that the edge of the viscous sublayer is positioned at $y=7\nu/u_\tau$ and the middle of the acoustic boundary layer as defined by Eq. (45) to be at $\delta_A/2=\sqrt{\nu/2\omega}$ he found this critical frequency to be approximately $\omega_*\approx 0.01u_\tau^2/\nu$. Introducing the normalised thickness of the acoustic boundary layer as $\delta_A^+=\delta_A/(\nu/u_\tau)=u_\tau\sqrt{2/(\nu\omega)}$ this critical condition appears when $\delta_A^+$ coincides with

$$\delta_{A,\mathrm{crit}}^+=\sqrt{2/0.01}\approx 14. \tag{50}$$

For the circular convective case there will be two slightly different critical conditions, obtained when the middle of the *convective* acoustic boundary layers $\delta_{A\phi M+}/2$ and $\delta_{A\phi M-}/2$, obtained from Eq. (49), are positioned at the edge of the viscous sublayer. This yields

$$\delta_{A\phi M\pm,\mathrm{crit}}/2=7\nu/u_\tau \tag{51}$$

or when normalised with $\nu/u_\tau$

$$\delta_{A\phi M\pm,\mathrm{crit}}^+=14 \tag{52}$$

which is approximately the same numerical value as in Eq. (50). Since $\delta_{A\phi M-}\neq\delta_{A\phi M+}$ when $M>0$ the critical frequency or Mach number will be different for waves travelling up- and downstream relative to the flow.

Howe proposed an extension of Prandtl's linear approximation for the turbulent eddy viscosity as [22]

$$\begin{aligned}\varepsilon_m&=0, \quad y<\delta_\nu(\omega)\\ &=\kappa u_\tau[y-\delta_\nu(\omega)], \quad y>\delta_\nu(\omega),\end{aligned} \tag{53}$$

where $\delta_\nu$ is a frequency-dependent thickness of the viscous sublayer. In order to match the experimental data obtained by Peters et al. [20] he suggested an empirical formula for $\delta_\nu$ as

$$\begin{aligned}\frac{\delta_\nu u_\tau}{\nu}&=\theta\left[1+\frac{\sigma(\omega/\omega_*)^3}{1+(\omega/\omega_*)^3}\right],\\ \omega_*\nu/u_\tau^2&\approx 0.01, \quad \omega>0,\end{aligned} \tag{54}$$

where $\theta=6.5$ and $\sigma=1.7$. Here, $\delta_\nu$ is approximately equal to the sublayer thickness for low frequencies when $\omega/\omega_*\to 0$ and increases to $\delta_\nu u_\tau/\nu=17.55$ when $\omega\gg\omega^*$ and the efficiency of the turbulence is reduced. A better alternative for Howe's

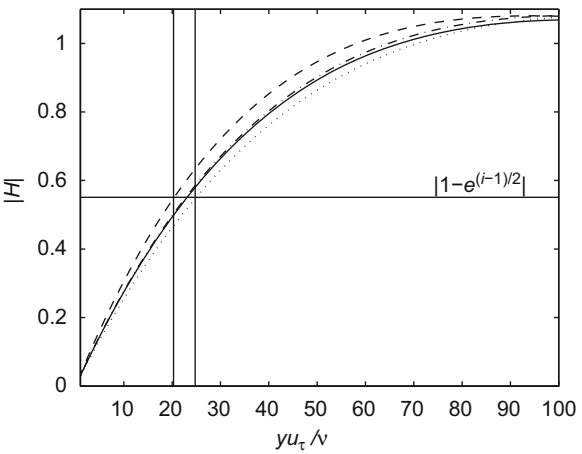


**Fig. 1.** Absolute value of normalised admittance for a circular tube with diameter=0.035 m, frequency=100 Hz and Mach number=0.2. —, Infinite plane, Eq. (44); – · – ·, cylindrical tube without flow, Eq. (48); – – –, cylindrical tube upstream, Eq. (48); · · ·, cylindrical tube downstream, Eq. (48). The two vertical lines represent the middle of the acoustical sublayer for the upstream and downstream cases (from left to right) calculated using Eq. (49). The coordinate $y$ represents the perpendicular distance to the wall.

empirical formula is to use $\delta^+_{A,\mathrm{crit}}$ instead of $\omega^*$ as the effect of the Mach number then is included. Consequently the following expression is obtained, which in principle is the same as recently was proposed by Dokumaci in Ref. [23],

$$\frac{\delta_\nu u_\tau}{\nu} = \theta\left[1+\frac{\sigma(\delta^+_{A,\mathrm{crit}}/\delta^+_A)^6}{1+(\delta^+_{A,\mathrm{crit}}/\delta^+_A)^6}\right], \quad \delta^+_{A,\mathrm{crit}} \approx 14, \quad \delta^+_A > 0, \tag{55}$$

where $\theta$ and $\sigma$ have the same numerical values as in Eq. (54). In order to match experimental data when using a solution strategy that takes into account the convective effects on the acoustic boundary layer the empirical expression (55) must be updated.

By averaging the momentum and continuity equations over the cross-sectional area and use the eddy viscosity to control the momentum and thermal boundary layers Howe could find an analytical expression for the wavenumber. The damping of the plane wave is given by the imaginary part of the wavenumber for the propagating wave as

$$\alpha_\pm = \frac{\sqrt{2\omega}}{c_0 2R(1\pm M)}\,real\left\{\sqrt{2}e^{-i\pi/4}\left[\frac{1}{(1\pm M)^2}\sqrt{\nu}F_A\left(\sqrt{\frac{i\omega\nu}{\kappa^2 u_\tau^2}},\delta_\nu\sqrt{\frac{i\omega}{\nu}}\right)\right.\right.$$
$$\left.\left.+\frac{\beta c_0^2}{C_p}\sqrt{\chi}F_A\left(\sqrt{\frac{i\omega\chi\xi^4}{\kappa^2 u_\tau^2}},\delta_\nu\sqrt{\frac{i\omega}{\chi}}\right)\right]\right\}, \tag{56}$$

where *real* indicates the real part, $\beta$ is the coefficient of expansion at constant pressure, $\chi = \kappa_{\mathrm{th}}/(\rho_0 C_p)$ is the thermometric conductivity and

$$F_A(a,b) = i\frac{H_1^{(1)}(a)\cos(b) - H_0^{(1)}(a)\sin(b)}{H_0^{(1)}(a)\cos(b) - H_1^{(1)}(a)\sin(b)}. \tag{57}$$

Here, $H_n^{(1)}$ is a Hankel function of order $n$.

### 3.3. The modified equation for conservation of momentum

Using the ideas from Ref. [22], based on augmenting the eddy viscosity $\varepsilon_m$ to the shear viscosity, the linear equation for conservation of momentum (10) in the axial direction is here modified to

$$\rho_0\frac{\mathrm{D}u_x'}{\mathrm{D}t} = -\frac{\partial p'}{\partial x} + \rho_0\nabla_\perp\{[\nu+2\varepsilon_m(r)]\nabla_\perp u_x'\}, \tag{58}$$

where $\mathrm{D}/\mathrm{D}t = \partial/\partial t + U_0\partial/\partial x$ is the linearized convective derivative, with the axial velocity $U_0$ equal to the incompressible mean flow velocity, and $\nabla_\perp$ is the nabla-operator taken over the cross-section of the duct. Expressed in cylindrical coordinates while assuming symmetric fields and harmonic waves [$\exp(i\omega t)$] Eq. (58) becomes

$$\left(i\omega + U_0\frac{\partial}{\partial x}\right)u_x' = -\frac{1}{\rho_0}\frac{\partial p'}{\partial x} + (\nu+2\varepsilon_m)\left(\frac{\partial^2 u_x'}{\partial r^2} + \frac{1}{r}\frac{\partial u_x'}{\partial r}\right) + 2\frac{\partial\varepsilon_m}{\partial r}\frac{\partial u_x'}{\partial r}. \tag{59}$$

The turbulent eddy viscosity spatial distribution in Eq. (53) expressed in cylindrical coordinates becomes

$$\varepsilon_m = \begin{cases} \kappa u_\tau[R-\delta_\nu(\omega)-r], & 0<r<R-\delta_\nu(\omega), \\ 0, & R-\delta_\nu(\omega)\le r<R. \end{cases} \tag{60}$$

Insertion of Eq. (60) into Eq. (59) yields for $0<r<R-\delta_\nu(\omega)$

$$\left(i\omega + U_0\frac{\partial}{\partial x}\right)u_x' = -\frac{1}{\rho_0}\frac{\partial p'}{\partial x} + [\nu+2\kappa u_\tau(R-\delta_\nu-r)]\left(\frac{\partial^2 u_x'}{\partial r^2} + \frac{1}{r}\frac{\partial u_x'}{\partial r}\right) - 2\kappa u_\tau\frac{\partial u_x'}{\partial r} \tag{61}$$

which after some rearrangements becomes

$$\left(i\omega + U_0\frac{\partial}{\partial x}\right)u_x' = -\frac{1}{\rho_0}\frac{\partial p'}{\partial x} + [\nu+2\kappa u_\tau(R-\delta_\nu)]\left(\frac{\partial^2 u_x'}{\partial r^2} + \frac{1}{r}\frac{\partial u_x'}{\partial r}\right) - 2\kappa u_\tau r\frac{\partial^2 u_x'}{\partial r^2} - 4\kappa u_\tau\frac{\partial u_x'}{\partial r}. \tag{62}$$

Insertion of Eqs. (16)–(18) into Eq. (62) yields

$$i\gamma(1-\Gamma M)u^* - i\Gamma p^* = \frac{\gamma}{s^2}\left[1+K_\nu\left(1-\frac{\delta_\nu}{R}\right)\right]\left(\frac{\partial^2 u^*}{\partial r^{*2}} + \frac{1}{r^*}\frac{\partial u^*}{\partial r^*}\right)$$
$$-K_\nu\frac{\gamma}{s^2}r^*\frac{\partial^2 u^*}{\partial r^{*2}} - 2K_\nu\frac{\gamma}{s^2}\frac{\partial u^*}{\partial r^*}, \tag{63}$$

where $K_\nu = 2\kappa u_\tau R/\nu$ has been introduced. The Galerkin procedure and the divergence theorem together with the boundary conditions in Eq. (24) applied to Eq. (63) yields the modified version of Eq. (31) as

$$\frac{\gamma}{s^2}\left[1+K_\nu\left(1-\frac{\delta_\nu}{R}\right)\right]\mathbf{B}\mathbf{u}^* - \frac{\gamma K_\nu}{s^2}\mathbf{B}_2\mathbf{u}^* + i\gamma(\mathbf{A}-\Gamma\mathbf{A}_m)\mathbf{u}^* - i\Gamma\boldsymbol{\varphi}p^* = \mathbf{0}, \tag{64}$$

where $\mathbf{B}_2$ is an $n\times n$ matrix, $n$ is the number of nodes and the $j$–$k$th component is given by

$$[\mathbf{B}_2]_{jk} = \int_0^1 \frac{\partial\phi_j}{\partial r^*}\frac{\partial\phi_k}{\partial r^*} r^{*2}\,\mathrm{d}r^*. \tag{65}$$

In a more compact form Eq. (64) can be written as

$$\frac{\gamma}{s^2}\mathbf{B}_u\mathbf{u}^* + i\gamma(\mathbf{A}-\Gamma\mathbf{A}_m)\mathbf{u}^* - i\Gamma\boldsymbol{\varphi}p^* = \mathbf{0}. \tag{66}$$

Here, $\mathbf{B}_u$ is an $n\times n$ matrix where $n$ is the number of nodes and the $j$–$k$th component is given by

$$[\mathbf{B}_u]_{jk} = \left[1+K_\nu\left(1-\frac{\delta_\nu}{R}\right)\right]\int_0^1 \frac{\partial\phi_j}{\partial r^*}\frac{\partial\phi_k}{\partial r^*} r^*\mathrm{d}r^* - K_\nu\int_0^1 \frac{\partial\phi_j}{\partial r^*}\frac{\partial\phi_k}{\partial r^*} r^{*2}\mathrm{d}r^*. \tag{67}$$

In the region $r > R-\delta_\nu(\omega)$ $\mathbf{B}_u$ is reduced to $\mathbf{B}$ as defined in Eq. (32).

### 3.4. The modified equation for conservation of energy

The influence of turbulence mixing on the energy equation was obtained in Ref. [22] by using Reynolds analogy. Here, the equation for conservation of energy (14) is modified accordingly; however, maintaining the effect of convection and the influence of a circular cross-section, and hence transfers to

$$\frac{\mathrm{D}T'}{\mathrm{D}t} - \frac{1}{\rho_0 C_p}\frac{Dp'}{Dt} = \nabla_\perp\cdot\left(\left[\chi+2\varepsilon_T(r)\right]\nabla_\perp T'\right) + \frac{2}{C_p}[\nu+2\varepsilon_m(r)]\frac{\partial U_0}{\partial r}\frac{\partial u_x'}{\partial r}, \tag{68}$$

where the eddy diffusivity is given by $\varepsilon_T(r) = \varepsilon_m(r)/\xi_t^2$. The turbulence Prandtl number is assumed to be constant; in air $\xi_t^2 \approx 0.7$. Substitution of the expression for the eddy diffusivity into Eq. (68) yields

$$\begin{aligned}\frac{\mathrm{D}T'}{\mathrm{D}t} - \frac{1}{\rho_0 C_p}\frac{\mathrm{D}p'}{\mathrm{D}t} = {}& \left[\chi + \frac{2\kappa u_\tau}{\xi_t^2}(R-\delta_\nu-r)\right]\left(\frac{\partial^2 T'}{\partial r^2}+\frac{1}{r}\frac{\partial T'}{\partial r}\right)\\ & - \frac{2\kappa u_\tau}{\xi_t^2}\frac{\partial T'}{\partial r} + \frac{2}{C_p}\left[\nu+2\kappa u_\tau(R-\delta_\nu-r)\right]\frac{\partial U_0}{\partial r}\frac{\partial u_x'}{\partial r},\end{aligned} \tag{69}$$

within $0 < r < R-\delta_\nu(\omega)$. This can be reformulated using the Prandtl number as

$$\begin{aligned}\rho_0 C_p\frac{\mathrm{D}T'}{\mathrm{D}t} - \frac{\mathrm{D}p'}{\mathrm{D}t} = {}& \kappa_{\mathrm{th}}\left[1+\frac{2\kappa u_\tau}{\nu}\frac{\xi^2}{\xi_t^2}(R-\delta_\nu-r)\right]\left(\frac{\partial^2 T'}{\partial r^2}+\frac{1}{r}\frac{\partial T'}{\partial r}\right)\\ & - \frac{\xi^2}{\xi_t^2}\kappa_{\mathrm{th}}\frac{2\kappa u_\tau}{\nu}\frac{\partial T'}{\partial r} + 2\rho_0\left[\nu+2\kappa u_\tau(R-\delta_\nu-r)\right]\frac{\partial U_0}{\partial r}\frac{\partial u_x'}{\partial r}.\end{aligned} \tag{70}$$

Introducing $K_t = K_\nu\xi^2/\xi_t^2$ Eq. (70) becomes

$$\begin{aligned}\rho_0 C_p\frac{\mathrm{D}T'}{\mathrm{D}t} - \frac{\mathrm{D}p'}{\mathrm{D}t} = {}& \kappa_{\mathrm{th}}\left[1+K_t\left(1-\frac{\delta_\nu}{R}\right)\right]\left(\frac{\partial^2 T'}{\partial r^2}+\frac{1}{r}\frac{\partial T'}{\partial r}\right) - \frac{\kappa_{\mathrm{th}}K_t}{R}r\left(\frac{\partial^2 T'}{\partial r^2}+\frac{1}{r}\frac{\partial T'}{\partial r}\right)\\ & - \frac{\kappa_{\mathrm{th}}K_t}{R}\frac{\partial T'}{\partial r} + 2\mu\left[1+K_\nu\left(1-\frac{\delta_\nu}{R}\right)\right]\frac{\partial U_0}{\partial r}\frac{\partial u_x'}{\partial r} - 2\mu K_\nu\frac{r}{R}\frac{\partial U_0}{\partial r}\frac{\partial u_x'}{\partial r}.\end{aligned} \tag{71}$$

Insertion of Eqs. (17) and (18) into Eq. (71) yields after some rearrangements

$$\begin{aligned}\frac{\gamma}{\gamma-1}\frac{1}{s^2\xi^2}\Bigg\{ & \left[1+K_t\left(1-\frac{\delta_\nu}{R}\right)\right]\left(\frac{\partial^2 T^*}{\partial r^{*2}}+\frac{1}{r^*}\frac{\partial T^*}{\partial r^*}\right) - K_t r^*\frac{\partial^2 T^*}{\partial r^{*2}} - 2K_t\frac{\partial T^*}{\partial r^*}\Bigg\} - \frac{i\gamma}{\gamma-1}(1-\Gamma M)T^*\\ & + i(1-\Gamma M)p^* + \frac{2\gamma}{s^2}\left[1+K_\nu\left(1-\frac{\delta_\nu}{R}\right)\right]\frac{\partial M}{\partial r^*}\frac{\partial u^*}{\partial r^*} - \frac{2\gamma K_\nu}{s^2}r^*\frac{\partial M}{\partial r^*}\frac{\partial u^*}{\partial r^*} = 0.\end{aligned} \tag{72}$$

The Galerkin procedure and the divergence theorem together with the boundary conditions in Eq. (24) applied to Eq. (72) yields the modified version of Eq. (34) as

$$\begin{aligned}\frac{\gamma}{\gamma-1}\frac{1}{s^2\xi^2}\Bigg\{\left[1+K_t\left(1-\frac{\delta_\nu}{R}\right)\right]\mathbf{B}\mathbf{T}^* - K_t\mathbf{B}_2\mathbf{T}^*\Bigg\} + \frac{i\gamma}{\gamma-1}(\mathbf{A}-\Gamma\mathbf{A}_m)\mathbf{T}^*\\ - \frac{2\gamma}{s^2}\left[1+K_\nu\left(1-\frac{\delta_\nu}{R}\right)\right]\mathbf{C}_m\mathbf{u}^* + \frac{2\gamma}{s^2}K_\nu\mathbf{C}_{m2}\mathbf{u}^* - i(\boldsymbol{\varphi}-\Gamma\boldsymbol{\varphi}_m)p^* = \mathbf{0},\end{aligned} \tag{73}$$

where $\mathbf{C}_{m2}$ is an $n \times n$ matrix, $n$ is the number of nodes and the $j$–$k$th component is given by

$$[\mathbf{C}_{m2}]_{jk} = \int_0^1 \phi_j \frac{\partial M}{\partial r^*} \frac{\partial \phi_k}{\partial r^*} r^{*2} \mathrm{d}r^*. \tag{74}$$

In a more compact form Eq. (73) becomes

$$\frac{\gamma}{\gamma-1}\frac{1}{s^2\xi^2}\mathbf{B}_T\mathbf{T}^* + \frac{i\gamma}{\gamma-1}(\mathbf{A}-\Gamma\mathbf{A}_m)\mathbf{T}^* - \frac{2\gamma}{s^2}\mathbf{C}_{mT}\mathbf{u}^* - i(\boldsymbol{\varphi}-\Gamma\boldsymbol{\varphi}_m)p^* = \mathbf{0}, \tag{75}$$

where $\mathbf{B}_T$ and $\mathbf{C}_{mT}$ are $n \times n$ matrices, $n$ is the number of nodes and the $j$–$k$th components are given by

$$[\mathbf{B}_T]_{jk} = \left[1 + K_t\left(1 - \frac{\delta_v}{R}\right)\right] \int_0^1 \frac{\partial \phi_j}{\partial r^*}\frac{\partial \phi_k}{\partial r^*} r^* \mathrm{d}r^* - K_t \int_0^1 \frac{\partial \phi_j}{\partial r^*}\frac{\partial \phi_k}{\partial r^*} r^{*2} \mathrm{d}r^* \tag{76}$$

and

$$[\mathbf{C}_{mT}]_{jk} = \left[1 + K_v\left(1 - \frac{\delta_v}{R}\right)\right] \int_0^1 \phi_j \frac{\partial M}{\partial r^*}\frac{\partial \phi_k}{\partial r^*} r^* \mathrm{d}r^* - K_v \int_0^1 \phi_j \frac{\partial M}{\partial r^*}\frac{\partial \phi_k}{\partial r^*} r^{*2} \mathrm{d}r^*, \tag{77}$$

respectively. In the region $r > R - \delta_v(\omega)$ $\mathbf{B}_T$ and $\mathbf{C}_{mT}$ are reduced to $\mathbf{B}$ and $\mathbf{C}_m$, respectively, as defined in Eqs. (32) and (35).

### 3.5. The modified finite element matrices

The modified version of the matrix equation (36) based on Eqs. (26), (66) and (75) becomes

$$\left[\begin{bmatrix} i/2 & \mathbf{0} & -i\boldsymbol{\varphi}^T \\ \mathbf{0} & \gamma\mathbf{B}_u/s^2 + i\gamma\mathbf{A} & \mathbf{0} \\ -i\boldsymbol{\varphi} & -\frac{2\gamma}{s^2}\mathbf{C}_{mT} & \frac{\gamma}{\gamma-1}\left[\frac{\mathbf{B}_T}{s^2\xi^2} + i\mathbf{A}\right] \end{bmatrix} - \Gamma \begin{bmatrix} i\overline{M}/2 & i\boldsymbol{\varphi}^T & -i(\boldsymbol{\varphi}_m)^T \\ i\boldsymbol{\varphi} & i\gamma\mathbf{A}_m & \mathbf{0} \\ -i\boldsymbol{\varphi}_m & \mathbf{0} & \frac{i\gamma}{\gamma-1}\mathbf{A}_m \end{bmatrix}\right] \begin{bmatrix} p^* \\ \mathbf{u}^* \\ \mathbf{T}^* \end{bmatrix} = \begin{bmatrix} 0 \\ \mathbf{0} \\ \mathbf{0} \end{bmatrix} \tag{78}$$

when $0 < r < R - \delta_v(\omega)$. Outside this region, when $R - \delta_v(\omega) < r < R$ only viscous and thermal effects exists and the problem is described by Eq. (36). An important feature of Eq. (78) is that the problem now must be updated for each new frequency or flow speed due to the variation of $\delta_v$.

## 4. Incompressible mean flow profile in tubes

The velocity profile of an incompressible mean flow in a tube is controlled by the Reynolds' number defined as

$$Re = \frac{2RU_0}{\nu}. \tag{79}$$

Experimental investigations have shown that the flow in a circular pipe is laminar if $Re < 2100$ [28] and that it is turbulent if $Re > 4000$. When $2100 < Re < 4000$ the flow experiences a transition, hence it can be either laminar or turbulent. A laminar flow profile is described by Poisson's equation, which can be solved analytically for circular tubes, yielding steady Hagen–Poiseuille flow as

$$M(r^*) = 2\overline{M}(1 - r^{*2}), \tag{80}$$

where $\overline{M}$ is the average mean flow over the entire cross-section. For turbulent pipe flow the distribution is much more complicated and can be approximated by Eqs. (41) and (40) in the turbulent region and in the viscous sublayer, respectively. Another widely accepted approximation of the turbulent mean flow distribution is the so-called seventh-root law for turbulent velocity distribution [28]. Based on experiments it has been shown that turbulent velocity profiles agree quite well with

$$\frac{U_0(r)}{U_0(0)} = \left(1 - \frac{r}{R}\right)^{1/n}, \tag{81}$$

where $n$=7 is representative value. Using the Mach number and its cross-sectional average this can also be written as

$$M(r) = \frac{60}{49}\overline{M}\left(1 - \frac{r}{R}\right)^{1/7}. \tag{82}$$

The velocity distribution within the viscous sublayer is of course not correct but in the main part of the tube this profile is a good approximation. The final expression for the length $\delta_v$ that is used in the FE-formulation will depend on what mean flow profile is assumed. The choice between how the relation is extracted and how it is used must hence be consistent.

For large values of the Reynolds number the mean velocity varies slowly in the core of the flow, as can be seen from Eq. (82), and is often approximated as being constant. In the model in Ref. [22] a constant flow profile was assumed when the convective momentum and continuity equations were combined to yield a non-homogenous wave equation from

which the wavenumber that yields the damping was calculated. The non-homogenous part is a result of the admittance of the wall shear layer that accounts for the interaction with the turbulent wall flow. The convective terms were discarded in the derivation of this wall admittance. In the FE-formulation in the present investigation an arbitrary mean flow profile can be used which opens the possibility to investigate the effect of using the constant flow profile or a more correct profile but also to include the effect of convection within the acoustic boundary layers.

## 5. Finite element models

The discretisation procedure for the proposed model is somewhat complicated since the element resolution must be dependent on the wavelength of the shear wave but also on the frequency and Mach number dependent thickness $\delta_\nu$. Hence, a new mesh will be required for every new flow speed or frequency. However, as the discretisation, for this axisymmetric case, is just in the radial direction it is a task that easily can be automated. The large gradients of the shear wave decays exponentially towards the centre of the tube and the region that needs the finest resolution is about one wavelength of the shear wave. If convective effects are neglected this shear wavelength can be estimated as [25]

$$\lambda = 2\pi\sqrt{2\nu/\omega}. \tag{83}$$

For the circular tube case, with a mean flow present, the wavelength will, as was shown earlier, be slightly different. In order to accurately resolve this region where most of the attenuation occurs, it was chosen to use a finer discretisation for $r$ limited by $R-3\pi\delta_{A\phi M\pm} < r < \mathrm{R}$, and resolve it with 15 second order elements. In the core region where $r < R-3\pi\delta_{A\phi M\pm}$ a biased mesh consisting of 20 second order elements is used in order to create a smooth transition to the small elements in the dense region from the much larger elements close to $r=0$ where the velocity gradient is close to zero. Validation of the mesh discretisation is carried out by comparison of the model for the case of no turbulence with the analytical solution by Dokumaci [9]. For a tube filled with air at room temperature, with diameter 0.035 m, at a frequency of 250 Hz and a mean flow varying between Mach=0.01 and 0.2 the relative error is less than 0.2% for the imaginary part of the wavenumber and even smaller for the real part. For the case with turbulence eddy viscosity the finite element mesh within $R-3\pi\delta_{A\phi M\pm} < r < \mathrm{R}$ is massaged so that the distance $\delta_\nu$ from $R$ falls at an element boundary. Additionally the mesh is slightly refined with some extra elements at the region close to $r=R-\delta_\nu$ where a discontinuity in the gradient of the acoustic particle velocity is enforced. For the flow cases in the following validation all appearances of $\delta_\nu$ falls within $R-3\pi\delta_{A\phi M\pm} < r < \mathrm{R}$. For any other case when $\delta_\nu > 3\pi\delta_{A\phi M\pm}$ the region $R-\delta_\nu < r < R-3\pi\delta_{A\phi M\pm}$ must also be refined in order to make sure that the shear wave is sufficiently described.

The solution of the eigenvalue problem given by Eq. (78) yields as many eigenvalues as there are degrees of freedom (twice the number of nodes +1). In Ref. [6] the modes are discussed and it was stated that the two modes that are least attenuated can be identified as representing acoustic waves. The other modes can be seen as representing thermal and hydrodynamic modes. For the present case, when the thermoviscous attenuation is smaller, due to higher Stokes numbers, the imaginary part of the wavenumber of the lowest of these higher modes might be of the same order of magnitude as for the ones representing acoustic waves. In order to find the acoustic waves the acoustic solutions will hence have to be sorted out using the real part of the wavenumber. The acoustic modes can easily be identified as they have a smaller real part of the wavenumber than all other modes. If the proposed model is used to extract a two-port that is coupled to other acoustic elements the near field effects or higher modes at the cross-section with a discontinuity might influence the results.

## 6. Model validation

### 6.1. Validation test cases

Three experimental test cases, reported by Peters et al. [20] and Allam and Åbom [21], have been used to validate the proposed numerical scheme. The test details are summarized in Table 1. The Stokes numbers are, as can be seen, rather high and hence the acoustic boundary layers can be considered as being thin. No experimental results for thick acoustic boundary layers have been found and the proposed model is so far only validated for thin layers. The measurements by Peters et al. [20] were used by Howe to validate his model in Ref. [22]; Allam and Åbom presented their measurements in Ref. [21] together with calculated data obtained using Howe's model. All three cases showed good correspondence with Howe's model except for some discrepancies for waves propagating towards the mean flow for low values of $\delta_A^+$. Possible reasons for those discrepancies were given by Howe [22] as anomalous experimental results or as a result from deviation from the eddy viscosity model due to a too small Reynolds number.

### 6.2. Inverse calculations

In order to identify the thickness $\delta_\nu$ (Eq. (53)), the proposed finite element scheme has been used to iteratively calculate the numerical value of $\delta_\nu$ that is required to match the available experimental data. The results, that have been achieved

both for the case of a flat mean flow profile as well as for a profile based on Eqs. (41) and (40), are shown in Figs. 2–5. The components in the system matrices in Eq. (78) were obtained using symbolical integration using the commercial software MAPLE 11 [31] leading to lengthy expressions that are not given here. For the constant mean flow profile the $\mathbf{C}_{mT}$-term vanishes but for the combined profile it will exist but turned out to be very difficult to calculate using MAPLE 11, hence it is neglected. The effect of this simplification is assumed to be small but needs to be further verified. It can be concluded that the deviations between the cases are not negligible; however, the largest deviations are focused to the measurements at 100 Hz from Ref. [21]. If this measurement were omitted the deviations would be much smaller. For values of $\delta^+_{A\phi M+}/\delta^+_{A\phi M\pm,\mathrm{crit}}$ less than or approximately equal to 0.9 it is not possible to find matching values in the downstream cases since the experimental damping is less than the purely viscothermal solution. If a curve similar to the one proposed by Howe (Eq. (55)) is assumed those values are, however, mainly important to get the slope of the relation correct. As long as the viscous sublayer covers the acoustic boundary layer the turbulence will hardly affect the damping at all and the damping will converge to the solution for thermoviscous bounded propagation proposed by Dokumaci [9]. The inversely obtained estimates of $\delta_\nu$ in the upstream direction do not follow the general trend outlined by Eq. (55) for values of $\delta^+_{A\phi M-}/\delta^+_{A\phi M\pm,\mathrm{crit}}$ less than or approximately equal to 0.9. The extra damping that yields this result was observed by Howe [22] in the measurements by Peters et al. [20] and was commented on as probably being anomalous. However, in the original experimental data by Allam and Åbom in Ref. [21], a similar trend can be found in both cases. So far, no explanation can be given for this extra damping caused by the very low Mach numbers, but the inversely obtained trend for $\delta_\nu$ is very similar for all three cases.

Since the data is not obtained at identical values for $\delta_A^+$ the cubic interpolation provided within the software package MATLAB [32] is used before averaging. The resulting average curves are shown in Fig. 6 and it is obvious that the numerical scheme that has been proposed cannot be combined with the empirical formula in Eq. (54) by Howe [22] since the convective effect in the boundary layers will require different values. It can also be seen that the effect of using the more

**Table 1**
Data for validation cases 1–3.

| | **Case 1** | **Case 2** | **Case 3** |
|---|---|---|---|
| **Author** | Peters et al. [20] | Allam and Åbom [21] | Allam and Åbom [21] |
| **Diameter (m)** | 0.030 | 0.035 | 0.035 |
| **Frequency (Hz)** | 88 | 100 | 250 |
| **Helmholtz no.** $[k_0R]$ | 0.024 | 0.032 | 0.080 |
| **Stokes no.** $[R\sqrt{\omega/\nu}]$ | 91 | 113 | 179 |
| **Mach no.** $[U_0/c_0]$ | 0.018–0.10 | 0.01–0.22 | 0.01–0.22 |
| **Reynolds no.** $\times\mathbf{10^3}[2RU_0/\nu]$ | 12–71 | 7.7–172 | 7.7–172 |
| $\delta_A^+\,[u_\tau\sqrt{2/(\nu\omega)}]$ | 3.5–31 | 3.1–48 | 2.0–31 |
| $\boldsymbol{k_0R/s}$ | 0.00027 | 0.00028 | 0.00045 |

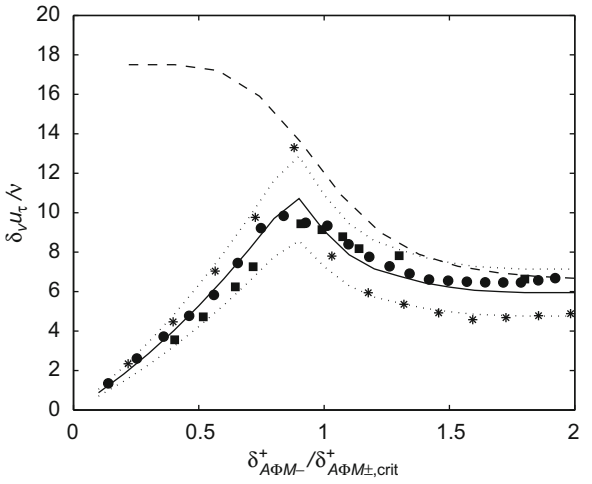


**Fig. 2.** Required $\delta_\nu u_\tau/\nu$ as a function of $\delta^+_{A\phi M-}/\delta^+_{A\phi M\pm,\mathrm{crit}}$ in the upstream direction when assuming constant flow distribution: (■) Peters et al. [20] $k_0R$=0.024; (∗) Allam and Åbom [21] $k_0R$=0.032; (●) Allam and Åbom [21] $k_0R$=0.080; (– – –) Empirical formula by Howe [22]; (—) average value; and (· · ·) ±20% of average value.

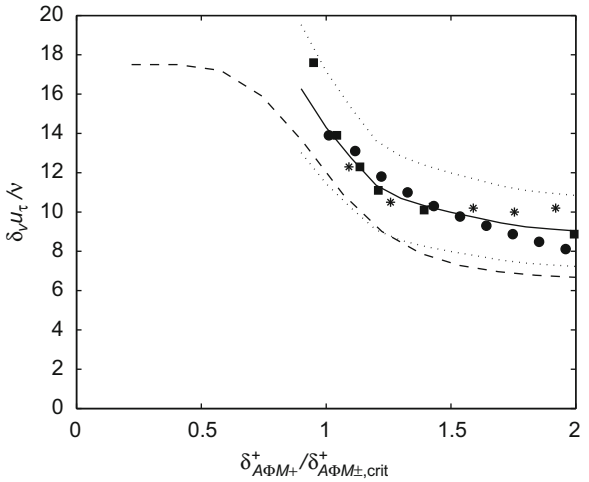


**Fig. 3.** Required $\delta_\nu u_\tau/\nu$ as a function of $\delta^+_{A\phi M+}/\delta^+_{A\phi M\pm,\mathrm{crit}}$ in the downstream direction when assuming constant flow distribution: (■) Peters et al. [20] $k_0R$=0.024; (∗) Allam and Åbom [21] $k_0R$=0.032; (●) Allam and Åbom [21] $k_0R$=0.080; (– – –) empirical formula by Howe [22]; (—) average value; and (· · ·) ±20% of average value.

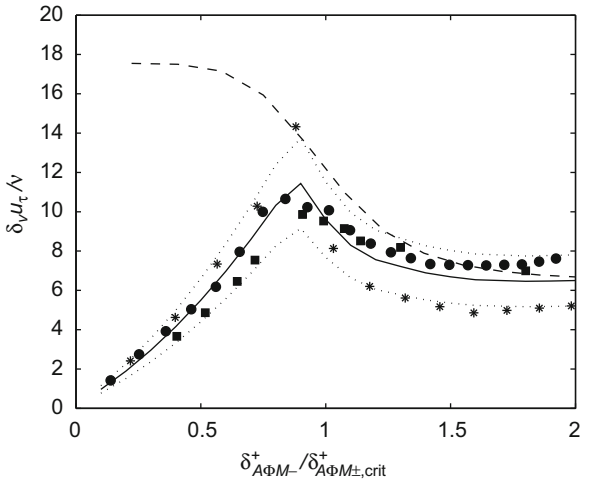


**Fig. 4.** Required $\delta_\nu u_\tau/\nu$ as a function of $\delta^+_{A\phi M-}/\delta^+_{A\phi M\pm,\mathrm{crit}}$ in the upstream direction when assuming turbulent flow distribution: (■) Peters et al. [20] $k_0R$=0.024; (∗) Allam and Åbom [21] $k_0R$=0.032; (●) Allam and Åbom [21] $k_0R$=0.080; (– – –) empirical formula by Howe [22]; (—) average value; and (· · ·) ±20% of average value.

complicated combined turbulent flow profile is quite small. The predicted values differs less than 10% compared to the flat profile predictions; the largest values appearing in the upstream direction. The combined profile yields, as expected due to the lower value of the spatial mean flow within the sublayer, solutions that are closer to the unconvected empirical formula in Eq. (55) by Howe. Since the calculations required when approximating the mean flow profile as constant are much simpler than those for the combined profile and the difference is rather small, only relations for the constant profile will be presented here.

Based on the observations above, a modified version of Howe's formula (55) is proposed here for calculations where the constant flow profile is used as

$$\frac{\delta_{\nu-}u_\tau}{\nu}=\theta_-\left[1+\frac{\sigma(\delta^+_{A\phi M\pm,\mathrm{crit}}/\delta^+_{A\phi M-})^7}{1+(\delta^+_{A\phi M\pm,\mathrm{crit}}/\delta^+_{A\phi M-})^7}\right],$$
$$\delta^+_{A\phi M-}>0,\quad \delta^+_{A\phi M\pm,\mathrm{crit}}=14 \tag{84}$$

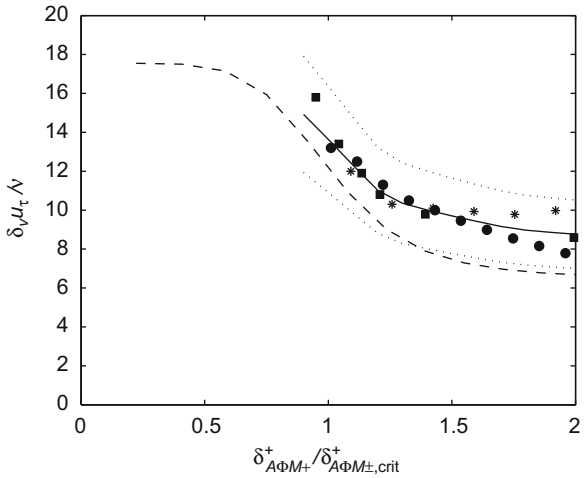


**Fig. 5.** Required $\delta_\nu u_\tau/\nu$ as a function of $\delta^+_{A\phi M+}/\delta^+_{A\phi M\pm,\mathrm{crit}}$ in the downstream direction when assuming turbulent flow distribution: (■) Peters et al. [20] $k_0R$=0.024; (∗) Allam and Åbom [21] $k_0R$=0.032; (●) Allam and Åbom [21] $k_0R$=0.080; (– – –) empirical formula by Howe [22]; (—) average value; and (· · ·) ±20% of average value.

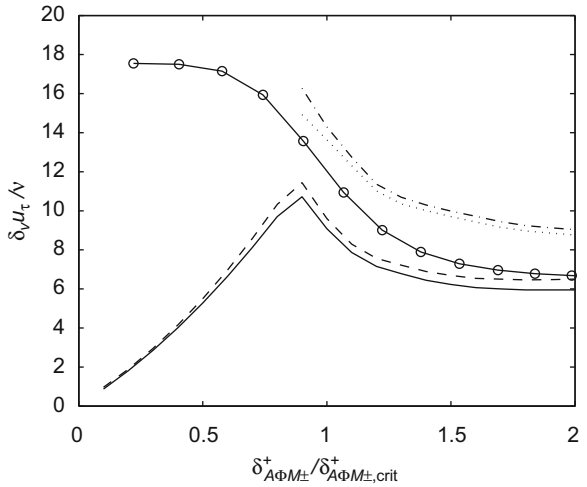


**Fig. 6.** Average required $\delta_\nu u_\tau/\nu$ as a function of $\delta^+_{A\phi M\pm}/\delta^+_{A\phi M\pm,\mathrm{crit}}$: (—) upstream, constant profile; (– – –) upstream, turbulent flow distribution; (– · – · ) downstream, constant profile; (· · ·) downstream, turbulent flow distribution; ⊖⊖⊖, Empirical formula by Howe [22].

and

$$\frac{\delta_{\nu+}u_\tau}{\nu}=\theta_+\left[1+\frac{\sigma(\delta^+_{A\phi M\pm,\mathrm{crit}}/\delta^+_{A\phi M+})^7}{1+(\delta^+_{A\phi M\pm,\mathrm{crit}}/\delta^+_{A\phi M+})^7}\right],\qquad \delta^+_{A\phi M+}>0,\quad \delta^+_{A\phi M\pm,\mathrm{crit}}=14 \tag{85}$$

for the upstream and downstream case, respectively. The constant $\sigma$ that controls the damping for low values of $\delta_{A\phi M\pm}$ is equal in both directions with a value $\sigma\approx1.2$ while $\theta_-\approx6$ and $\theta_+\approx9$, that controls the damping when the turbulent damping is dominant is different for up- and downstream propagating waves. Predictions based on Eqs. (84) and (85) are shown in Figs. 7–9 for the three validation cases. The predictions of the part of the curves where the turbulent damping dominates are of similar accuracy as those from using the model by Howe [22] in the downstream direction. The backward wave predictions from the proposed model deviates in a similar way as was predicted by Dokumaci in Ref. [23] from those from using Howe's model.

In order to predict the, so far unexplained, extra damping appearing when $\delta^+_{A\phi M-}/\delta^+_{A\phi M\pm,\mathrm{crit}}<0.9$ in the upstream case, it is also proposed to use the lowest value of

$$\frac{\delta_{\nu-}u_\tau}{\nu}=\theta_{-,\mathrm{eng}}\left[\left(\frac{\delta^+_{A\phi M-}}{\delta^+_{A\phi M\pm,\mathrm{crit}}}\right)^{1.5}+1\right] \tag{86}$$

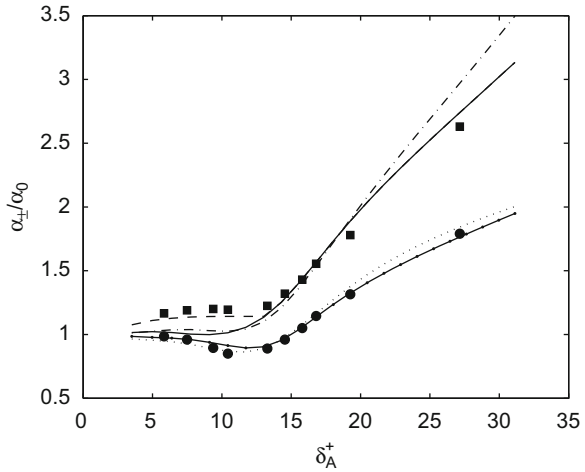


**Fig. 7.** Relation between damping and normalised acoustic boundary layer for $k_0R$=0.024: (■) experimental, upstream [20]; (●) experimental, downstream [20]; (– · – · ) Howe [22], upstream; (· · · ) Howe [22], downstream; (—) present model, upstream; ●—●—●, Present model, downstream; and (– – –) present model, low Mach number correction, upstream.

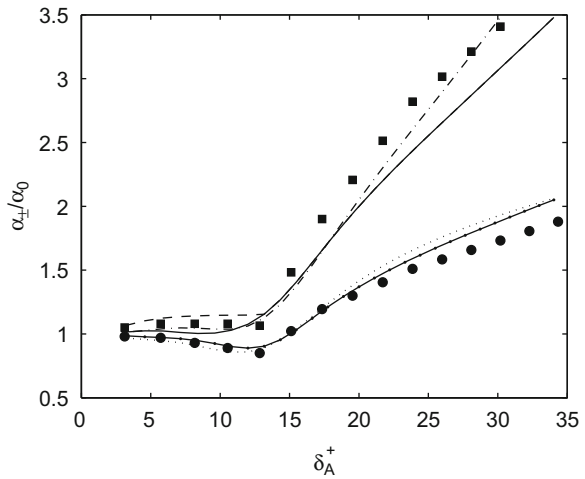


**Fig. 8.** Relation between damping and normalised acoustic boundary layer for $k_0R$=0.032: (■) experimental, upstream [21]; (●) experimental, downstream [21]; (– · – · ) Howe [22], upstream; (· · · ) Howe [22], downstream; (—) present model, upstream; ●—●—●, Present model, downstream; and (– – –) present model, low Mach number correction, upstream.

and Eq. (84) for engineering purposes. The constant $\theta_{-,\mathrm{eng}} \approx 11.7$ yields the best correspondence with the available experimental data.

Fig. 10 shows the same relations as in Fig. 7 but zoomed in on the region dominated by the thermoviscous boundary effects. Here, it can be seen that the proposed numerical model converges to the Dokumaci solution [9] for a thermoviscous, non-turbulent, bounded fluid while the solution by Howe [22] is slightly different. This is most likely due to the $1/s^2$ term in the Kirchhoff damping that is neglected in Howe's model. This effect is very small for large Stokes numbers but gets more important for smaller when the acoustic boundary layers gets thicker.

The purpose of this study is to propose a method to treat situations where the acoustic boundary layers are thicker than those present in the experimental studies in Refs. [20,21], where the shear wavenumber $s$ is larger than 90 (see Table 1). To the authors' knowledge no such high quality experimental data, i.e., with shear wavenumbers much smaller than 90, is available in the literature. The experimental data in Ref. [24] for a charge air cooler includes shear wavenumbers in the domain $6 \leq s \leq 35$, which is much smaller than the data from Refs. [20,21] used in this paper. However, the presented transmission loss data represents a complete charge air cooler which is a built-up component that has been assembled by two irregularly shaped volumes with plastic walls and a matrix of narrow cooling tubes. This experimental data will hence not provide a reliable validation case for the waveguide model that has been proposed in the present study. In order to get an impression of how the proposed model behaves for smaller Stokes numbers, the damping from an imaginary case where the diameter of the duct is smaller and the Stokes number is 40 is shown in Fig. 11. This is of course not a validation of the

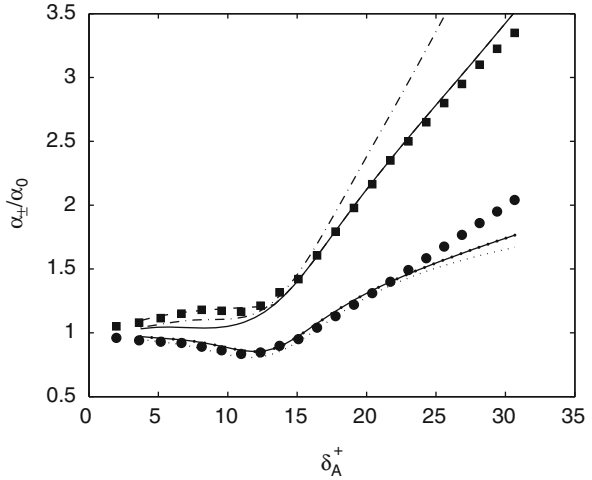


**Fig. 9.** Relation between damping and normalised acoustic boundary layer for $k_0R$=0.080: (■) experimental, upstream [21]; (●) experimental, downstream [21]; (– · – ·) Howe [22], upstream; (· · ·) Howe [22], downstream; (—) present model, upstream; ●—●—●, present model, downstream; and (– – –) present model, low Mach number correction, upstream.

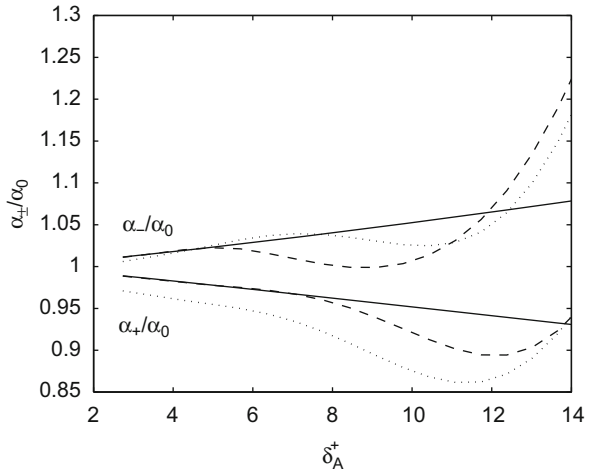


**Fig. 10.** Calculated damping coefficient $\alpha_\pm/\alpha_0$ as a function of $\delta_A^+$ for $k_0R$=0.024: (—) model by Dokumaci [9]; (· · ·) model by Howe [22]; and (– – –) predicted by proposed model.

model since no experimental data exists, but it can be seen that the damping still converges towards the viscous solution by Dokumaci [9] as expected for low values of $\delta_A^+$ while the estimates from using the model by Howe now is much less accurate. It should be noticed here that the damping in the upstream direction is calculated using Eq. (84). In the inverse calculations it was shown that Eq. (86) would give the best predictions and yield more damping than the thermoviscous solution. This investigation still gives no explanation for this damping and physical considerations as well as further measurements are required in order to explain but also to verify if this additional damping is present for smaller values of the Stokes number.

## 7. Application example—simple tube

From practical point of view it might be interesting to study the attenuation for a fixed geometry as a function of frequency or Mach number. In order to visualize the difference between the proposed model and the model by Howe [22] three single ducts with the diameters 30, 15 and 3 mm are analyzed using a fixed flow speed ($M$=0.1) and a frequency

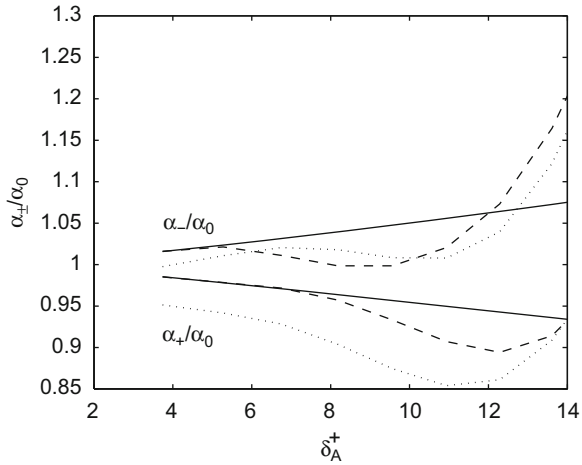


**Fig. 11.** Calculated damping coefficient $\alpha_{\pm}/\alpha_0$ as a function of $\delta_A^+$ for $k_0R$=0.011: (—) model by Dokumaci [9]; ( · · · ) model by Howe [22]; and ( – – – ) predicted by proposed model.

**Table 2**
Data for application case 1–4.

| | Case 1 | Case 2 | Case 3 | Case 4 |
|---|---|---|---|---|
| **Diameter (m)** | 0.030 | 0.015 | 0.003 | 0.003 |
| **Frequency (Hz)** | 50–1000 | 50–1000 | 50–1000 | 50–1000 |
| **Helmholtz no.** $[k_0R]$ | 0.014–0.28 | 0.0069–0.14 | 0.0014–0.028 | 0.0014–0.028 |
| **Stokes no.** $[R\sqrt{\omega/\nu}]$ | 69–307 | 35–153 | 6.9–31 | 6.9–31 |
| **Mach no.** $[U_0/c_0]$ | 0.1 | 0.1 | 0.1 | 0.06 |
| **Reynolds no.** $\times 10^3[2RU_0/\nu]$ | 68 | 34 | 6.8 | 4.1 |
| $\boldsymbol{k_0R/s \times 10^{-4}}$ | 2–9 | 2–9 | 2–9 | 2–9 |

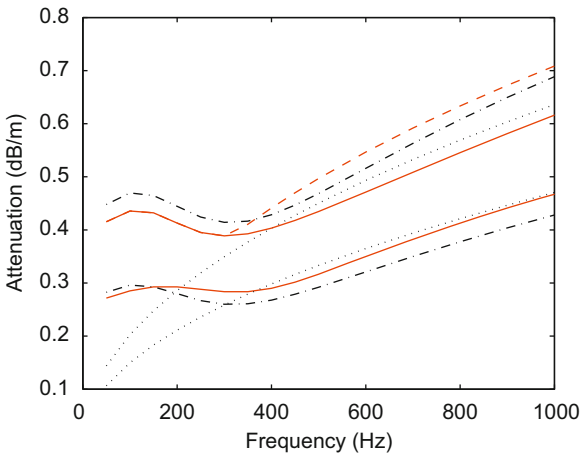


**Fig. 12.** Predicted attenuation for a single tube with diameter 30 mm at $M$=0.1. Upper curves correspond to the upstream case: ( – · – · ) Howe [22]; ( · · · ) Dokumaci [9]; (—) present model Eq. (84) or Eq. (85); ( – – – ) present model Eq. (86).

sweep between 50 and 1000 Hz. The duct with the smallest diameter is additionally analyzed using a smaller Mach number. Air at room temperature is assumed and important figures are summarized in Table 2.
The predicted attenuation is shown in Figs. 12–15 for Cases 1–4, respectively. The definition for attenuation is here

$$\text{attenuation} = 8.686\left|\text{Im}(k_0\Gamma)\right| (\text{dB}/m). \tag{87}$$

The differences between those from the proposed model and those from the model by Howe are relatively small for wider tubes as can be seen in Figs. 12 and 13. The differences are, as expected, increasing with decreasing diameter. For the tube

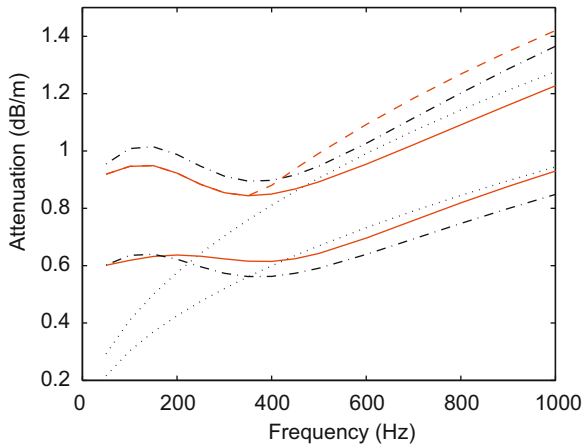


**Fig. 13.** Predicted attenuation for a single tube with diameter 15 mm at $M$=0.1. Upper curves correspond to the upstream case: (– · – · ) Howe [22]; (· · · ) Dokumaci [9]; (—) present model Eq. (84) or Eq. (85); and (– – – ) present model Eq. (86).

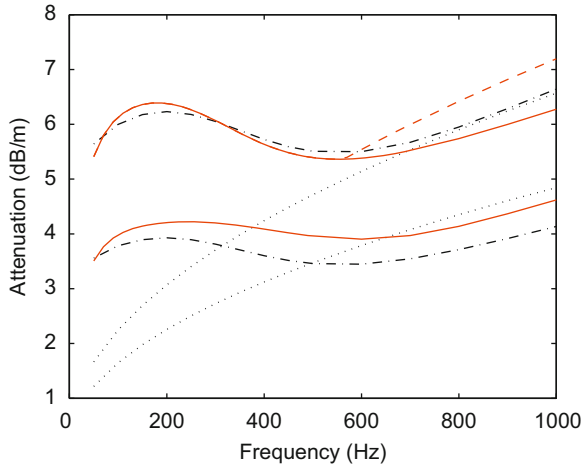


**Fig. 14.** Predicted attenuation for a single tube with diameter 3 mm at $M$=0.1. Upper curves correspond to the upstream case: (– · – · ) Howe [22]; (· · · ) Dokumaci [9]; (—) present model Eq. (84) or Eq. (85); and (– – – ) present model Eq. (86).

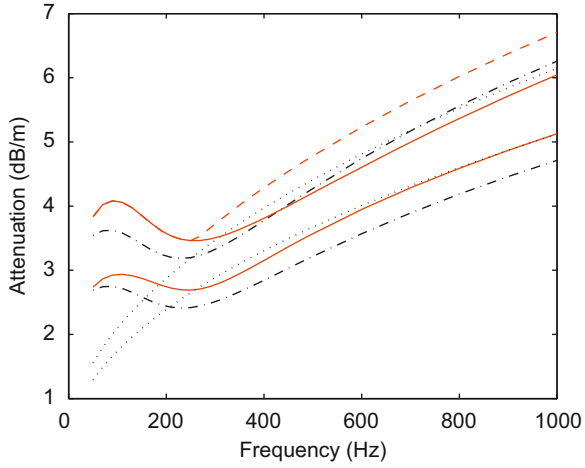


**Fig. 15.** Predicted attenuation for a single tube with diameter 3 mm at $M$=0.06. Upper curves correspond to the upstream case: (– · – · ) Howe [22]; (· · · ) Dokumaci [9]; (—) present model Eq. (84) or Eq. (85); and (– – – ) present model Eq. (86).

with the diameter 3 mm are the differences of the order 0.5 dB/m. Important is that these differences also depends strongly on the Mach number, which can be seen in Figs. 14 and 15. This result can be explained by the influence of the Mach number on the sublayer thickness.

## 8. Summary and conclusions

A numerical model that predicts the damping due to the interaction between turbulence and sound waves propagating in a tube has been proposed and validated. It consists of an extension of the finite element scheme proposed by Astley and Cummings in Ref. [6] in combination with the turbulent eddy viscosity model proposed by Howe in Ref. [22]. The formulation is carried out using cylindrical coordinates and allows convection of an arbitrary flow profile. Three cases from the literature, with different duct diameters and frequencies, have been used for validation. It has been shown that the accuracy is of the same order as the model proposed by Howe in Ref. [22] for intermediate Stokes numbers ($\sim$100) and Mach numbers less than 0.1. However, the proposed model shows better correspondence with the pure thermoviscous predictions obtained from the model proposed by Dokumaci [9] for low Mach numbers. An empirical model for engineering purposes has been proposed for the unexplained additional damping observed in all three validation cases for low Mach numbers in the upstream direction.

The development of the proposed numerical scheme involves some simplifications that can be addressed in order to further improve the accuracy of the predictions. Important are most likely the influence of the neglected radial velocity and the assumption of a constant pressure over the cross-section. Several authors have dealt with this problem (see e.g. Refs. [7,8]) for the purely thermoviscous bounded case and have shown that the simplification will most likely have a noticeable, but small effect. However, it is not clear in how large extent it will affect this model where the turbulence is included.

The turbulence eddy viscosity model that has been used is, as was stated by Howe in Ref. [22], based on the work by Prandtl and is indeed very simplified. The spatial distribution that was proposed by Howe enforces a discontinuity in the gradient of the total viscosity at the position given by $\delta_\nu$. The numerical scheme proposed here gives the possibility to use a more advanced turbulence model that better takes into account the properties of the transition between the turbulent region and the viscous sublayer. Also the value of the Reynolds number is important since there will be a lower limit when the model is valid. In Ref. [22] it was stated that the eddy viscosity model might be questionable for situations where the Reynolds number is less than $10^4$.

Finally, the model needs to be validated using experimental data for more values on the Stokes number. Particularly at low Stokes numbers, where the acoustic boundary layers are thick, more experimental data is required. It would also be beneficial to include the model by Dokumaci [23], which should be valid for thicker sublayers than the model by Howe [22], in the validation since it provides a simpler treatment of the problem than the model proposed in the present paper. Although it is not valid for such thick sublayers as the proposed model it might provide useful estimates with less computational effort.

## Acknowledgements

The work described in this paper was funded by Volvo Car Corporation, EMFO – the Swedish Emission Research Programme and KTH CICERO – Centre for Internal Combustion Engine Research Opus. This funding is gratefully acknowledged by the authors. Dr. Sabry Allam provided the original measurement data from Ref. [21] and is also acknowledged.

## References

[1] G. Kirchhoff, Uber den einfluss der wärmteleitung in einem gas auf die schallbewegung, *Annalen der Physik und Chemie* 134 (6) (1868) 177–193.
[2] C. Zwikker, C.W. Kosten, in: *Sound Absorbing Materials*, Elsevier, Amsterdam, 1949.
[3] H. Tijdeman, On the propagation of sound waves in cylindrical tubes, *Journal of Sound and Vibration* 39 (1) (1975) 1–33.
[4] K.S. Peat, A first approximation to the effects of mean flow on sound propagation through cylindrical capillary tubes, *Journal of Sound and Vibration* 175 (4) (1994) 475–489.
[5] J.–G. Ih, C.–M. Park, H.–J. Kim, A model for sound propagation in capillary ducts with mean flow, *Journal of Sound and Vibration* 190 (2) (1996) 163–175.
[6] R.J. Astley, A. Cummings, Wave propagation in catalytic converters: formulation of the problem and finite element solution scheme, *Journal of Sound and Vibration* 188 (5) (1995) 635–657.
[7] K.–W. Jeong, J.–G. Ih, A numerical study on the propagation of sound through capillary tubes with mean flow, *Journal of Sound and Vibration* 198 (1) (1996) 67–79.
[8] M. Willatzen, Phase shift and attenuation characteristics of acoustic waves in a flowing gas confined by cylindrical walls, *Journal of Sound and Vibration* 261 (2003) 791–804.
[9] E. Dokumaci, Sound transmission in narrow pipes with superimposed uniform mean flow and acoustic modelling of automobile catalytic converters, *Journal of Sound and Vibration* 182 (5) (1995) 799–808.
[10] E. Dokumaci, On transmission of sound in circular and rectangular narrow pipes with superimposed mean flow, *Journal of Sound and Vibration* 210 (3) (1998) 375–389.
[11] K.S. Peat, Convected acoustic wave motion along a capillary duct with an axial temperature gradient, *Journal of Sound and Vibration* 203 (5) (1997) 855–866.

[12] K.S. Peat, R. Kirby, Acoustic wave motion along a narrow cylindrical duct in the presence of an axial mean flow and temperature gradient, *Journal of the Acoustical Society of America* 107 (4) (2000) 1859–1867.
[13] E. Dokumaci, An approximate dispersion equation for sound waves in a narrow pipe with ambient gradients, *Journal of Sound and Vibration* 240 (4) (2001) 637–646.
[14] S.F. Tardu, G. Binder, R.F. Blackwelder, Turbulent channel flow with large-amplitude velocity oscillations, *Journal of Fluid Mechanics* 267 (1994) 109–151.
[15] A. Scotti, U. Piomelli, Numerical simulation of pulsating turbulent channel flow, *Physics of Fluids* 13 (5) (2001) 1367–1384.
[16] P. Comte, M. Haberkorn, G. Bouchet, V. Pagneaux, Y. Aurégan, Large-eddy simulation of acoustic propagation in a turbulent channel flow, in: E. Lamballais, R. Friedrich, B.J. Geurts, O. Métais (Eds.), *Direct and Large-Eddy Simulation VI*, 2006, pp. 521–528.
[17] U. Ingard, V.K. Singhal, Sound attenuation in turbulent pipe flow, *Journal of the Acoustical Society of America* 55 (3) (1974) 535–538.
[18] D. Ronneberger, C.D. Ahrens, Wall shear stress caused by small amplitude perturbations of turbulent boundary-layer flow: an experimental investigation, *Journal of Fluid Mechanics* 83 (3) (1977) 433–464.
[19] R.R. Mankbadi, J.T.C. Liu, Near-wall response in turbulent shear flows subjected to imposed unsteadiness, *Journal of Fluid Mechanics* 238 (1992) 55–71.
[20] M.C.A.M. Peters, A. Hirschberg, A.J. Reijnen, A.P.J. Wijnands, Damping and reflection coefficient measurements for an open pipe at low Mach and low Helmholtz numbers, *Journal of Fluid Mechanics* 256 (1993) 499–534.
[21] S. Allam, M. Åbom, Investigation of damping and radiation using full plane wave decomposition in ducts, *Journal of Sound and Vibration* 292 (2006) 519–534.
[22] M.S. Howe, The damping of sound by wall turbulent shear layers, *Journal of the Acoustical Society of America* 98 (3) (1995) 1723–1730.
[23] E. Dokumaci, On attenuation of plane sound waves in turbulent mean flow, *Journal of Sound and Vibration* 320 (2009) 1131–1136.
[24] M. Knutsson, M. Åbom, Sound propagation in narrow tubes including effects of viscothermal and turbulent damping with application to charge air coolers, *Journal of Sound and Vibration* 320 (2009) 289–321.
[25] S. Temkin, in: *Elements of Acoustics*, Acoustical Society of America, 2001.
[26] A.D. Pierce, in: *Acoustics – An Introduction to Its Physical Principles and Applications*, Acoustical Society of America, New York, 1994.
[27] O.C. Zienkiewics, R.L. Taylor, in: *The Finite Element Method*, fourth ed., McGraw-Hill, New York, 1990.
[28] J.K. Vennard, R.L. Street, in: *Elementary Fluid Mechanics*, Wiley, New York, 1982.
[29] J.O. Hinze, in: *Turbulence*, McGraw-Hill, New York, 1975.
[30] H. Schlichting, in: *Boundary Layer Theory*, McGraw-Hill, New York, 1979.
[31] *Maple 11, User's Manual*, Waterloo Maple, 2007.
[32] *Matlab 7, User's Manual,* MathWorks, 2007.